NJC

Accepted Manuscript

This is an *Accepted Manuscript*, which has been through the Royal Society of Chemistry peer review process and has been accepted for publication.

Accepted Manuscripts are published online shortly after acceptance, before technical editing, formatting and proof reading. Using this free service, authors can make their results available to the community, in citable form, before we publish the edited article. We will replace this *Accepted Manuscript* with the edited and formatted *Advance Article* as soon as it is available.

You can find more information about *Accepted Manuscripts* in the Information for Authors.

Please note that technical editing may introduce minor changes to the text and/or graphics, which may alter content. The journal's standard Terms & Conditions and the Ethical guidelines still apply. In no event shall the Royal Society of Chemistry be held responsible for any errors or omissions in this *Accepted Manuscript* or any consequences arising from the use of any information it contains.

ROYAL SOCIETY OF CHEMISTRY

www.rsc.org/njc

NJC

RSCPublishing

LETTER

Photoluminescence properties of $BaSiF_6$: Eu^{3+}, Eu^{3+}/K^+ and Eu^{3+}/Tb^{3+} co-doped phosphors

Cite this: DOI: 10.1039/c3nj00000x

Yuan Zhang,[a] Long Yuan,[a] Keke Huang,[a] Yanyan Du,[b] and Shouhua Feng[a*]

Received 00th XXXXX 2013,
Accepted 00th XXXXX 2013

DOI: 10.1039/c3nj00000x

www.rsc.org/njc

A series of $BaSiF_6$-based rare-earth down-converting phosphors have been firstly hydrothermally prepared and characterized. Under ultraviolet radiation excitation, $BaSiF_6$:Eu^{3+} phosphors show the characteristic f-f transition of Eu^{3+} and give a bright orange-red emission. We found the luminescence quenching concentration was 15%, which is relatively high. To further enhance the luminescence, K^+ was added in as charge compensator. Furthermore, cold white colour can be obtained by co-doping Tb^{3+} ions.

Recently, a few potential candidates as luminescent materials have been explored,[1,2]such as tungstates[3] and tantalates.[4] Among them, fluoride have unique optical properties such as high chemical stability and good solid solubility.[5] Low-energy phonons and high iconicity endow fluoride with lower quenching probability of the excited states.[6] Recently, Adachi's group reported a series of Mn-activated $XSiF_6$ (X= NH_4, K, Zn, Ba) as excellent red phosphors for application in WLED.[7-15] $BaSiF_6$, with hexagonal crystal structure, crystallizes in a trigonal symmetry with the space group $R\bar{3}m$ have attracted significant interest.[8] Some other hexafluorosilicate such as $ZnSiF_6$:Mn^{4+} [9-10] and similar structure $BaTiF_6$:Mn^{4+} [11] have also been investigated. Furthermore, K_2TiF_6:Mn^{4+} show great promise as a commercial red phosphor in warm white LEDs.[12] Therefore, complex fluorine open up new avenues for high efficient phosphors.

Recently, up-conversion Pr^{3+} doped $BaSiF_6$ and Yb^{3+}/Tm^{3+} co-doped $BaSiF_6$ have also been reported.[13] Unfortunately, so far little attention has been paid to rare-earth down-converting luminescent properties of $BaSiF_6$ host matrix. Considering that Eu^{3+} ions have been widely used as classical luminescent activator for many commercial phosphors such as $Y(V,P)O_4$:Eu^{3+},Y_2O_3:Eu^{3+}, and Y_2O_2S:Eu^{3+}. From the viewpoint of this, we doped Eu^{3+} and other ions (K^+ and Tb^{3+}) to reveal the process of down-converting luminescence in the hexafluorosilicate material.

In this work, we report an efficient one-step hydrothermal method using hydrated silica and NH_4HF_2 as the metal chelating agent for the preparation of a series of Eu^{3+} doped $BaSiF_6$ needle-like phosphors. We attributed the relatively high quenching concentration to the long atomic distance between activators which are occupied the Ba sites. To further enhance the photoluminescence (PL) intensities, we tried a coating process in previous work,[14] therefore, we added K^+ as the charge compensator this time and discussed the corresponding luminescence properties. These assemblies exhibit a needle-like appearance. Moreover, through co-doping of Eu^{3+} and Tb^{3+} ions and changing of the doping ratio, we obtain a cold-white colour emission.

Power XRD patterns of $BaSiF_6$: xEu^{3+}(x=0-0.2) samples are shown in **Fig. 1**. All the samples matched well with JCPDS card number 15-0736 ($BaSiF_6$), demonstrating our synthesized phosphor belongs to the space group of D^5_{3d}-$R\bar{3}m$ (trigonal).[15][16] The introduction of dopants does not make any significant changes to the host.[17] In $BaSiF_6$, Ba-atom at a site of D_{3d} point symmetry and is coordinated by 12 F^- ions at an average distance of 285.9 pm. The small Si^{4+} atoms are coordinated octahedrally by 6 F^- ions.[18] **Fig. 2 (a)-(d)** shows the structure and coordination environments of $BaSiF_6$. Considering the ionic radius and the charge, the Eu^{3+} is expected to substitute the Ba^{2+} sites in the $BaSiF_6$ crystal structure (Ba^{2+}=135Å, Eu^{3+}=95Å). We also co-doped K^+ into the $BaSiF_6$:xEu^{3+} as charge compensating agent. (Its XRD pattern is listed in the supporting information **Fig. S1(a)**.)

Fig. 3 (a) and (b) show SEM images of the $BaSiF_6$ host material. In **Fig. 1**, the relative Bragg reflection peak intensity of (110) is obviously dominated which has good agreement with the large quantity of needle-like appearance. Their lengths range from several micrometers to tens of micrometers. There also exist many fragments in the SEM image, we assume most of that owing to the etching by HF, thus the uniform microneedles can

be etched into imhomogeneous.[19] To further prove this assumption, we used $Ba(NO_3)_3$ instead of $Ba(OH)_2$ to synthesize $BaSiF_6$, since the volume of HF can be reduced to 3-4 drops, the SEM image is listed in **Fig. 3 (b)**. (Its XRD pattern is listed in **Fig. S1(c)**.) From which we can see the microneedles appearance is much more homogeneous. High-resolution TEM image shown in **Fig. 3 (c)** reveal the distance between the adjacent atomic lattice is 0.285 nm, which is in good agreement with the lattice spacing in the (021) planes of trigonal $BaSiF_6$ (0.2845 nm, JCPDS card number 15-0736). To investigate whether the dopant will influence the morphology, we also listed the SEM images of Eu^{3+}/K^+ and Eu^{3+}/Tb^{3+} doped samples in the **Fig. S2**. From those images, we can see no obviously difference in the doped samples.

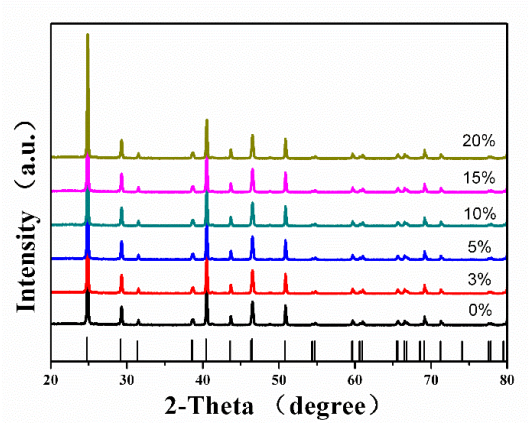

Fig. 1 XRD patterns of $BaSiF_6$ host material and $BaSiF_6$:xEu^{3+} (x=0%, 3%, 5%, 10%, 15%, 20%) phosphors. The black vertical lines at the bottom indicate the standard XRD pattern of $BaSiF_6$ (JCPDS card number 15-0736).

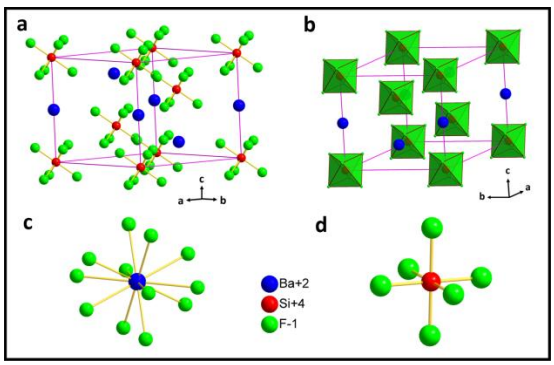

Fig. 2 (a and b) Unit cell representation of the crystal structure of $BaSiF_6$. Blue, red, and green spheres represent Ba, Si, and F atoms, respectively. Barium and silicon sites are described by (c) and (d), respectively.

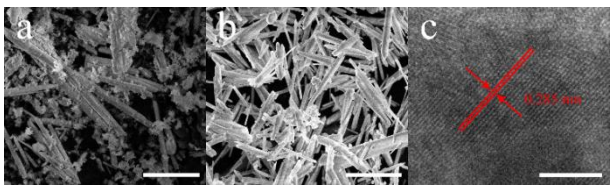

Fig. 3 SEM images of $BaSiF_6$. a) Synthesized with $Ba(OH)_2$ and 25 drops HF. b) Synthesized with $Ba(NO_3)_2$ and c) 3 drops HF. The scale bar is 10 μm in a) and b). High-resolution TEM image showing well-defined (021) lattice fringes of $BaSiF_6$ with a *d* spacing of 0.285 nm. The scale bar is 5 nm in c).

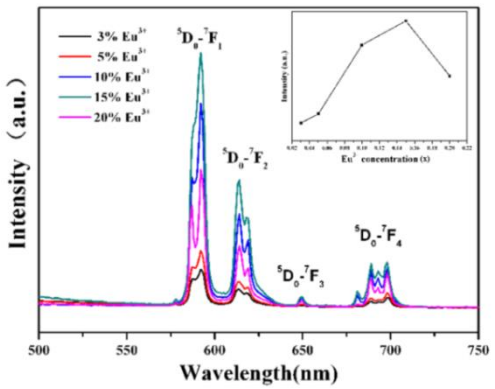

Fig. 4 Room temperature DC emission spectra of BaSiF6:xEu^{3+}(x=0-0.2). The insert image shows the intensity dependences of doping contents at 592 nm for $BaSiF_6$:Eu^{3+}. All spectra were recorded under 395 nm excitation of a 450 W Xe lamp.

Fig. 4 depicts the emission spectra of the $BaSiF_6$: xEu^{3+} micro-phosphors by the excitation at 395 nm. The sharp peaks at 550-750 nm are ascribed to the characteristic intra-configurational $4f^6$-$4f^6$ transitions of Eu^{3+} in the host: $^5D_0$-^7F_j (j=1-4). The dominant one is the $^5D_0$-$^7F_1$ magnetic dipole transition with inversion symmetry at 592 nm, which is consistent with the D_{3d} point symmetry of Ba ions.

The relation between PL intensity of $BaSiF_6$:Eu^{3+} phosphors and Eu^{3+} ion doping concentration at 592 nm are shown in **Fig. 4** (insert). It can be seen that the optimal doping concentration of Eu^{3+} is ~15 mol%. Along with the increase of the concentration of Eu^{3+}, the distance between luminescence centers decreases which makes the non-radiative energy transfer between Eu^{3+}-Eu^{3+} ions come more easily.[20] However, when the luminescence centers grow in a certain number, they are too close to each other in the lattice. Ion-ion interaction, accompanied by the cross-relaxation energy transfer and non-radiative relaxation make luminescent intensity decrease, then occurs to concentration quenching.[21] It should be noted that this quenching concentration is relatively high while most quenching concentration occurs at 5 mol%-8 mol%.[22] We assumed that whether the high covalency of Si-F bond or the structural features of $BaSiF_6$ such as long Eu-Eu distances (476.4 pm) may result in difficulty in energy transfer.[23]

In $BaSIF_6$ host matrix, the unequivalence doping comes into being vacancy defects [$V``_{Ba}$]. Since the ionic radius of K^+ (138 pm) is similar to that of Ba^{2+} (135 pm), it may not disturb the crystal lattice of the host. Therefore, K^+ was added in the same molar weight as Eu^{3+} to act as the charge compensators to enhance the PL intensities of the Eu^{3+}-doped phosphors. (Its XRD pattern is listed in **Fig. S1(a)** .) **Fig. 5** shows the room temperature emission spectra of the $BaSiF_6$:Eu^{3+} and $BaSiF_6$:Eu^{3+}/K^+ phosphors. (The excitation spectra and decay patterns are shown in **Fig. S7**. The SEM mapping images of $BaSiF_6$:15%Eu^{3+}/15%K^+ are listed in the **Fig. S3**.) As shown in **Fig. 5**, these two emission spectra have similar features, but the

luminescence density is increased by about 58.7% with the addition of K^+.[24] K^+ introduced a positive charge and acted as a charge compensator. With its chemical nature of low oxidation states and distinct ionic radii, K^+ usually used to modify the local site symmetry of Eu^{3+} and gave the best improvement in the alkaline-earth phosphors.[24,25,26] Since, the vacancy defects [$V``_{Ba}$] of the phosphors decrease, the luminescence increases. We calculated the ratios of the integral area of intensity of the $^5D_0$-$^7F_1$ transition to the $^5D_0$-$^7F_2$ transition, and found that the ratio of the $BaSiF_6$:Eu^{3+} (1.738) is slightly smaller than that of $BaSiF_6$:Eu^{3+}/K^+ (1.744). It indicated that K doping can modify the local site symmetry of Eu^{3+} which may be the reason for the enhanced emissions.[24] Further tuning of the PL intensities of this family of crystals by co-doping with other ions is expected.

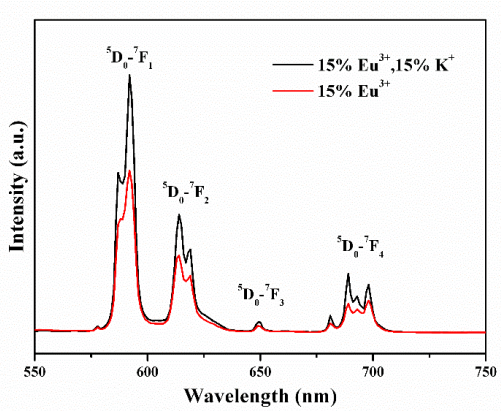

Fig. 5 Room temperature PL emission spectra of $BaSiF_6$: 15% Eu^{3+} and $BaSiF_6$: 15% Eu^{3+}, 15%K^+. All spectra were recorded under 395 nm excitation of a 450 W Xe lamp.

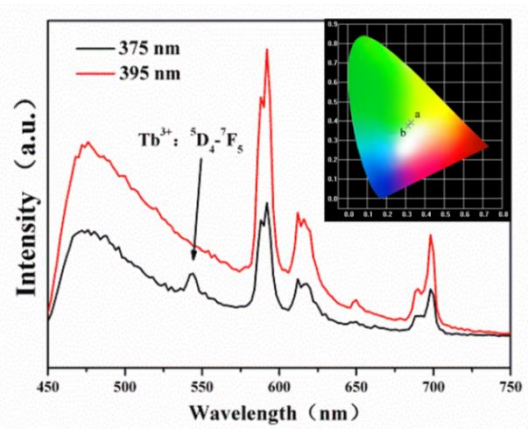

Fig. 6 PL emission spectra of $BaSiF_6$:3%Eu^{3+}, 2%Tb^{3+} under 395 nm (red) and 375 nm (black) excitation. The insert image is the CIE color coordination of $BaSiF_6$: 3%Eu^{3+}, 2%Tb^{3+} under 395 nm (a) and 375 nm (b) excitation.

The energy transfer from Tb^{3+} to Eu^{3+} in the $BaSiF_6$:Eu^{3+}, Tb^{3+} co-doped samples has been observed in the photoluminescence spectra. We synthesized a series of $BaSiF_6$:15%Tb^{3+}, xEu^{3+} (x=2%, 5%, 10%, 15%, 20%) phosphors. (The XRD data are shown in the **Fig. S1(d)**.) **Fig. S4(a)** shows the emission spectra which consist of f-f transition of Tb^{3+} and Eu^{3+}. The four main peaks located at 544 nm, 592 nm, 616 nm, 698 nm are belong to Tb^{3+} ($^5D_4$-$^7F_5$), Eu^{3+} ($^5D_0$-$^7F_1$), Eu^{3+} ($^5D_0$-$^7F_2$), Eu^{3+} ($^5D_0$-$^7F_4$), respectively. **Fig. S4(b)** shows the emission intensities of Tb^{3+} and Eu^{3+} as a function of the Eu^{3+} doping concentration in $BaSiF_6$. It shows the major characteristic emission of Tb^{3+} (544 nm, $^5D_4$-$^7F_5$) decreased all the time. The Eu^{3+} emission (592nm, $^5D_0$-$^7F_1$) should increase at first then decrease due to the concentration quenching effect. However, there is a fall in our profile when the Eu^{3+} concentration is 10 mol% which makes the proof of energy transfer not sufficient. Therefore, we listed the excitation and emission spectra of $BaSiF_6$:15%Tb^{3+}, 15%Eu^{3+} monitored under different conditions to further confirm the energy transfer. **Fig. S5(a)** exhibits the excitation spectra of $BaSiF_6$:15%Tb^{3+}, 15%Eu^{3+} under different emission wavelengths monitored. Under 592 nm (Eu^{3+}, $^5D_0$-$^7F_1$), excitation peaks of both Eu^{3+} and Tb^{3+} can be detected, especially the one at 394 nm (Eu^{3+}, $^7F_0$-$^5L_6$). However, under 544 nm (Tb^{3+}, $^5D_4$-$^7F_5$), the peak at 394 nm disappeared. **Fig. S5(b)** exhibits the emission spectra of $BaSiF_6$:15%Tb^{3+}, 15%Eu^{3+} under different excitations. Upon 394 nm excitation (Eu^{3+}, $^7F_0$-$^5L_6$), there is only the emission of Eu^{3+}, and the positions of peaks are as same as those in **Fig. 4**. Under 351 nm excitation (Tb^{3+}, $^7F_6$-$^5D_2$), emission of both Eu^{3+} and Tb^{3+} can be detected. Since there is no absorption of Eu^{3+} at 351 nm, we can conclude the energy of Eu^{3+} emission comes from the absorption of Tb^{3+}. The presence of the excitation peaks of Tb^{3+} (317 nm, $^7F_6$-$^5D_0$; 351 nm, $^7F_6$-$^5D_2$; 361 nm, $^7F_6$-$^5G_5$; 375 nm, $^7F_6$-$^5G_6$) in the excitation spectrum monitored with Eu^{3+} emission (592nm, $^5D_0$-$^7F_1$) also indicates the energy transfer process (**Fig. S5(a)**).

Fig. 6 shows PL emission spectra of $BaSiF_6$:3%Eu^{3+}, 2%Tb^{3+} under 375 and 397 nm light excitation, respectively. (**Fig. S8** shows the PL excitation spectra of $BaSiF_6$:Eu^{3+}, Tb^{3+}.) Besides the characteristic emission of Tb^{3+} and Eu^{3+}, there is an obviously emission ranging from 450 nm to 530 nm, peaking at 470 nm. We ascribed this emission to the non-bridging oxygen hole centers which can also be described as $SiOH \rightarrow SiO\bullet + \bullet H$ (dots represent unpaired electrons).[27] The excitation and emission spectra have been shown in the supporting information **Fig. S6**. We assumed that the photoluminescence of host material is derived from the oxygen hole. Note that because of the weak PL intensity of the oxygen hole centers compared with the Eu^{3+}, this emission band did not appear when the concentration of rare earth activator is relative high.

When Eu^{3+} and Tb^{3+} are co-doped into $BaSiF_6$ host, we achieved the colour-tunable luminescence since Eu^{3+} gives an orange-red emission and Tb^{3+} gives a green-blue one.[7] CIE colour coordinations are (0.3284, 0.3922), (0.3122, 0.3753) under 395 nm and 375 nm excitation, respectively (**Fig. 6**(insert)). These two sets CIE coordination are very close to the white light, and both are very attracted cold-white light emission. The CCT are 5642 K and 6267 K.

In summary, a series of $BaSiF_6$:xEu^{3+} (x=3%, 5%, 10%, 15%, 20%), $BaSiF_6$:15%Eu^{3+}/15%K^+ and $BaSiF_6$: 3%Eu^{3+}, 2%Tb^{3+} phosphors are synthesized via a one-step hydrothermal synthesis. Their structural and luminescence properties are investigated. Upon excitation with n-UV light of 395 nm, these phosphors show bright orange-red emissions peaking at 592 nm

due to the $^5D_0$-$^7F_1$ transition of Eu^{3+}. Emission intensity of $BaSiF_6$:Eu^{3+} phosphor was significantly enhanced by doping charge compensation K^+. With Eu^{3+} and Tb^{3+} co-doping, due to energy transfer process, we obtain a cold-white PL emission. CIE colour coordination are (0.3284, 0.3922), (0.3122, 0.3753) under different excitation light which are both very close to the standard white light.

Experimental

The initial chemicals in this work, $Ba(OH)_2$ (99.99%), H_2SiO_3•xH_2O (99.99%), NH_4HF_2 (99.99%), HF (AR grade), $Eu(NO_3)_3$ (99.9%), $Tb(NO_3)_3$ (99.9%) and $Ba(NO_3)_2$ (99.99%), were purchased from Sinopharm Chemical Reagent Co., Ltd, China. All of the chemicals were used as received without further purification.

A series of $BaSiF_6$ samples were all prepared *via* a one-step hydrothermal synthesis. In a typical synthesis process, 1 mmol $Ba(OH)_2$ [or $Ba(NO_3)_2$] and 2 mmol NH_4HF_2 were added into a Teflon vessel. To investigate the optimum synthesis condition, SiO_2•xH_2O was varying from 0.4 g to 0.9g, and the volume of HF varied from 5 drops to 30 drops. The concentration of HF plays an important role in obtaining a pure phase of red phosphor $BaSiF_6$, the final PH value should be between 3 and 4. The stoichiometric solutions of $Eu(NO_3)_3$ [and $Tb(NO_3)_3$] were fully mixed together with the above mixture. The Teflon vessel was enclosed in the stainless steel autoclave with 80% capacity, and kept at 180 °C for 72 h. It was then cooled to room temperature naturally. The resulting products were then collected by filtration, washed with deionized water for several times till the pH reached at 7, and dried in air atmosphere at 60 °C for 6 h.

The phase purity and crystallinity of the samples were examined by powder X-ray diffraction (XRD) performing on a Rigaku D/max 2550 diffractometer with a graphite monochromator using CuKα radiation (λ = 1.5418 Å) operating at 50 kV and 200 mA at room temperature by step scanning in the angle range of 20° ≤ 2θ ≤ 80° with increments of 0.02°. Scanning electron microscope (SEM) images were recorded with a Helios NanoLab 600i Dual Beam System, FEI Company, America. The emission and excitation spectra of the phosphors were recorded using an Edinburgh Instruments FLS 920 spectrofluorimeter equipped with a continuous 450 W xenon lamp and using a R928 photomultiplier tube detector. Lifetime measurements were performed using the same spectrophotometer and detectors using a 100 W pulsed xenon lamp μF920H (200-900 nm, 10-100 Hz).

Acknowledgement

This work was supported by National Natural Science Foundation of China (Grants 90922034, 21131002 and 21201075), the Specialized Research Fund for the Doctoral Program of Higher Education (SRFDP Grant 20110061130005) and Graduate Innovation Fund of Jilin University (Grant 2015143).

Notes and references

a State Key Laboratory of Inorganic Synthesis and Preparative Chemistry, College of Chemistry, Jilin University, Changchun, 130012, P. R. China. Email: shfeng@jlu.edu.cn; Fax: +86-431-85168624; Tel. +86-431-85168661.
b Shanghai Institute of Ceramics, Chinese Academy of Sciences, 200050 Shanghai, P. R. China.

1 M. Shang, C. Li, and J. Lin, *Chem. Soc. Rev.*, 2014, **43**, 1372.
2 J. Zhou, Q. Liu, W. Feng, Y. Sun, and F. Li, *Chem. Rev.*, 2015, **115**, 395.
3 Y. Du, Y. Zhang, K. Huang, S. Wang, L. Yuan and S. Feng, *Dalton Trans.*, 2013, **42**, 8041.
4 J. Yu, K. Huang, L. Yuan and S. Feng, *New J. Chem.*, 2014, **38**, 1441.
5 L. Ge, L. Yuan, K. Huang, W. Feng, H. Fang and S. Feng, *New J. Chem.*, 2015, **39**, 5080.
6 Y. P. Du, X. Sun, Y. W. Zhang, Z. G. Yan, L. D. Sun and C. H. Yan, *Cryst. Growth Des.*, 2009, **9**, 2013.
7 Y. K. Xu and S. Adachi, *J. Electrochem Soc.*, 2012, **159**, E11.
8 D. Sekiguchi and J. Nara, S. Adachi, *J. Appl. Phys.*, 2013, **113**, 183516.
9 H. Ryosuke and S Adachi, *ECS J. Solid Stste Sc.*, 2014, **3**, R144.
10 H. Ryosuke and S. Adachi, *J. Appl. Phys.*, 2013, **114**, 213502.
11 D. Sekiguchi and S. Adachi, *ECS J. Solid Stste Sc.*, 2014, **3**, R60.
12 H. Zhu, C. Lin, W. Luo, S. Shu, Z. Liu, Y. Liu, J. Kong, E. Ma, Y. Cao, R. Liu and X. Chen, *Nat Commun.*, 2014, **5**, 4312.
13 E. van der Kolk, P. Dorenbos, C. van Eijk, A. Vink, C. Fouassier and F. Guillen, *J. Lumin.*, 2002, **97**, 212.
14 Y. Zhang, W. Feng, K. Huang, L. Yuan, Y. Du, X. Wu, S. Feng, *Eur. J. Inorg. Chem.*, 2015, **4**, 690.
15 B. F. Hoskins, A. Linden, P. C. Mulvaney and T. A. O'Donnell, *Inorg. Chim. Acta*, 1984, **88**, 217.
16 G. Svensson, J. Albertsson, C. Svensson and L. I. Elding, *Acta Chem. Scand.*,1986, **40a**, 631.
17 H. L. Jeong and Y. D. Huh, *Chem. Lett.*, 2010, **39**, 34.
18 G. Wang, W. Qin, D. Zhang, G. Wei, K. Zheng, L. Wang and F. Ding, *J. Fluorine Chem.*, 2009, **130**, 755.
19 X. Jiang, Y. Pan, S. Huang, X. Chen, J. Wang and G. Liu, *J. Mater. Chem. C*, 2014, **2**, 2301.
20 R. Cao, G. Chen, X. Yu, C. Cao, K. Chen, P. Liu and S. Jiang, *J. Solid State Chem.*, 2014, **220**, 97.
21 X. Jiang, Y. Pan, S. Huang, X. Chen, J. Wang and G Liu, *J. Mater. Chem. C*, 2014, **2**, 2301.
22 Shili Gai, Chunxia Li, Piaoping Yang and Jun Lin, *Chem. Rev.*, 2014, **114** (4), 2343.
23 Grant C. Bleier, May Nyman, Lauren E.S. Rohwer and Mark A. Rodriguez, *J. Solid State Chem.*, 2011, **184**, 3221.
24 X. Zhao, Y. Ding, Z. Li, T. Yu and Z. Zou, *J. Alloys Compd.*, 2013, **553**, 221.
25 Z. Mu, Y. Hu, L. Chen and X. Wang, *J. Electrochem. Soc.*,2011, **158**, J287.
26 J. Liu, X. D. Wang, Z. C. Wu and S. P. Kuang, *Spectrochim Acta A Mol Biomol Spectrosc*, 2011, **79**, 1520.
27 C. Zhang and J. Lin, *Chem. Soc. Rev.*, 2012, **41**, 7938.

